An analytical model for high velocity impacts on thin CFRPs woven laminated plates

J. López-Puente, R. Zaera, C. Navarro *

Carlos III University of Madrid, Department of Continuum Mechanics and Structural Analysis, Avda. de la Universidad 30, 28911 Leganes, Madrid, Spain

Abstract

An analytical model to study the impact process of a spherical projectile penetrating at high velocity into a carbon/epoxy plain woven laminate is developed in this work. The model is based on an energy balance, where the kinetic energy of the projectile is absorbed by the laminate by three different mechanisms: laminate crushing, linear momentum transfer and tensile fiber failure. A non-homogeneous differential equation is obtained. A subsequent simplification using regular perturbation analysis gives a closed-form solution that allows the approximative calculation of the residual velocity and hence the ballistic limit. The model is validated with the results of experimental tests in which the residual velocity is measured by means of high speed cameras.

Keywords: Composites; Ballistic; Analytical model; Impact

1. Introduction

New requirements of strength, stiffness and lightness in structural components have brought an upsurge in the sphere of composite materials. The technical development of these components has come mainly from the aeronautical and aerospatial industries which impose very strict criteria in the material selection, particularly with regard to their density since any slight reduction of the total mass of the structure means a saving of power and of fuel. The composite materials most used for structural applications in these sectors are of laminated carbon fiber in an epoxy matrix which combines good mechanical properties, high resistance to corrosion and fatigue, and low density ($\rho \sim 1400\ \mathrm{kg/m^3}$). Before designing a structural component of this carbon fiber/epoxy laminate, its mechanical behavior should be know for the load conditions to which it will be subjected in service. These kind of laminates perform well under plane or bending stresses, whether static or alternating stresses, but they show lower strength to perpendicular impact. These impacts can fracture the continuity between plies and may cause other damage that is not visible to the naked eye and which may

* Corresponding author. Tel.: +34 91 624 9491; fax: +34 91 624 9430.
E mail address: navarro@ing.uc3m.es (C. Navarro).

spread beyond the impact zone. The speed of the reduction of the residual properties by these cracks under alternating stress is an additional hazard, and impacts are not infrequent. The horizontal stabilizer of a commercial plane, often made of carbon/epoxy fiber, may be impacted by a projectile or by hailstones during landing/takeoff or in flight; a satellite in orbit or a space shuttle by any of the innumerable small items of orbital debris. It is obvious, therefore, the correct design of certain carbon/epoxy laminates, high-speed impact should be taken into account.

The first experimental studies of the behavior of composite materials against ballistic impact were made in the 60s (see the excellent revisions by Abrate (1991, 1994)). This type of investigation was mainly for the military in the 70s, and the documentation was secret until the end of the 80s when several studies were published, such as that of Vasudev and Meehlman (1987) of the ballistic behavior of glass fiber laminates in epoxy and vinylester matrices. Cantwell (1988) published an analysis of the damage to carbon/epoxy laminates over a wide range of impact velocities, from 10 to 500 m/s, the effect being measured by ultrasonic non-destructive inspection. This last study was among the first to show the effects of the localization of the damage and its extent for different laminate thicknesses. Fuji et al. (2002), verified for CFRPs specimens, that at higher velocities the extension of the damage decreases and, Kim et al. (2003), carried out impact tests with hailstones on quasi-isotropic carbon/epoxy panels, identifying the various mechanism of damage at each velocity. Other publications reported ballistic impact results on tubes of this material (Tennyson and Lamontagne, 2000; Will et al., 2002). Their objective was to analyze two effects: by one side the damage on the first laminate that receives the impact, and on the other hand the effect produced both by the projectile and the detached fragments on the inner face of the same tube. This was important in view of the number of double-walled aeronautical and aerospatial structural components made of carbon/epoxy. Another important topic for the design of these components is that they may be subjected to very low temperatures in service, such as airplanes (-60 °C) and spacecrafts (-150 °C). Studies on this subject were carried out by López-Puente et al. (2002) showing how the temperature and the type of reinforcement (tape or woven) affect the size of the damage area of CFRPs when subjected to high velocity impacts.

Numerical simulations of the problem require the use of three-dimensional finite element or finite differences codes, given the anisotropic nature of the composite laminates, and they involve high computational costs. With two-dimensional axisymmetric models the computer time is shorter and the simplified hypotheses adopted, as regards the mechanical behavior of the material, may still provide reasonably accurate predictions. Nandlall et al. (1998) used the finite element explicit code LS-DYNA 2D to predict the extension of the various types of damage caused by the impact of fragments on glass/polyester laminates, ignoring the anisotropy of the laminates since the structural response was mainly local. Another way to diminish the computation time is to discretize the laminate in an axisymmetric configuration using one-dimensional elements, reducing the degrees of freedom of the model. Sun and Potti (1996) predicted ballistic limits and the post-impact residual velocities of the projectile by using a model with two-node finite element (axial symmetry), and two degrees of freedom per node. Fully three-dimensional simulations, such as those presented by López-Puente et al. (2003), included a modeling of the effect of impact on CFRP laminates. Chen et al. (1997) used an interesting methodology for their simulations of high-speed impact (up to 500 m/s) of fragments on carbon/epoxy laminates; they used Smoothed Particle Hydrodynamics (SPH) for the spatial discretization, a method that had been developed at the end of the 70s to solve problems of astrophysics and of the collision of sub-atomic particles and then extended to the Mechanics of Solids.

There are also analytical models based on an analysis of the global response of each system and the application of principles of moment conservation or of energy balance. These analysis provide algebraic or differential equations whose solutions are of value in the early stages of the design process of structural components. Most of these models have been developed in the sphere of ballistic protection, using flexible laminates of aramid or polyethylene fibers (Chocrón et al., 1997; Navarro, 1998; Naik and Doshi, 2005; Naik et al., 2005, 2006). A smaller number of impact models consider glass fiber or carbon laminates whose structural function is to resist static or dynamic loads and that may be subjected to high-speed impact. Other studies have appeared (Wen, 2001; Ben-Dor et al., 2002; Ulven et al., 2003) that apply models developed for isotropic materials (generally metallic), where the composite being homogenized to give effective properties. The necessary simplifications to take into account in analytical models means that they are useful only for the problem for which they were derived. In all the analytical models so far described, in which the deforma-

tion and damage mechanisms are specific to composite materials, the most often quoted is that of ballistic impact on CFRP beams developed by Cantwell and Morton (1985, 1990). Despite its relative simplicity it provides, with acceptable accuracy, the force needed to perforate laminates up to 4 mm thick. It assumes that the kinetic energy of the projectile is dissipated by four processes of fracture or deformation: local bending, deformation by contact, delamination and finally expulsion of the plug. In thicker laminates, the hypothesis of fracture is no longer adequate since it overestimates the energy dissipated in the plug exit. In 1990, the same researchers published modifications of their original model, rejecting the energies of bending and contact.

This paper proposes an analytical model to predict the residual velocity of a spherical projectile after impacting at ballistic velocity regime against carbon/epoxy plain woven laminates. This simulation tool, based on energetic criteria, may be used whether or not the laminate is perforated. It is a low-cost model and its predictive capacity is adequate at early stages of the design process.

2. Model description

The analytical model is formulated in terms of energy balance. In this type of carbon/epoxy reinforcement it is considered that the kinetic energy of the projectile E_k will be absorbed by the laminate by three different processes: laminate breakage due to crushing E_c, linear momentum transferred from the projectile to the detached part of laminate E_m, and tensile fiber failure breakage E_f. Elastic deformations contribution is usually neglected in analytical impact models because of the low amount of energy accumulated by this kind of deformation as compared to other breakage processes. This last means that no consideration of the elastic waves propagation is required by the model for brittle materials (Zukas, 1982); nevertheless, elastic wave propagation phenomena have to considered in the modelization of fabric flexible laminates submitted to impact. The energy absorbed by delamination neither was considered due to the low extension of this type of damage in plain woven laminates (López-Puente et al., 2002) and its low specific energy. Plastic deformation of the projectile has also been neglected, because it has been experimentally observed for this type of materials that it does not suffer any permanent strains. Every energy absorption mechanisms above-mentioned varies with time and their sum must be equal to the kinetic energy lost by the projectile at each instant.

The mathematical formulation of this energy balance constitutes the fundamental equation for the analytical model. The basic balance equation of the problem may be written as

$$-\mathrm{d}E_k = \mathrm{d}E_c + \mathrm{d}E_m + \mathrm{d}E_f \tag{1}$$

A spatial rather than temporal integration was chosen because the expressions are considerably simplified. Following the analysis of each energetic term of Eq. (1) is presented:

- *Kinetic energy of the projectile*: Let x be the variable that describes the position of the projectile, from the upper side of the composite laminate (Fig. 1). Between two positions (x and $x + \mathrm{d}x$) the bullet will lose a quantity of energy given by

$$\mathrm{d}E_k(x) = \frac{1}{2} m_p \, \mathrm{d}(v(x)^2) \tag{2}$$

  in which m_p is the projectile mass, that remains constant along the process, and v its velocity, which varies with the position. As indicated above, this energy variation is absorbed by the laminate by three different mechanisms, once the projectile strikes against the composite plate.
- *Energy absorbed by laminate crushing*: When the projectile contacts the laminate it breaks the composite material in front of it by compression. Between two different positions of the projectile, x and $x + \mathrm{d}x$, the energy dissipated by this mechanism was estimated as the product of the out-of-plane compressive strength of the laminate σ_c multiplied by the distance covered by the bullet, $\mathrm{d}x$. Fig. 2 shows a sketch of this process. The corresponding energetic term may be written as follows:

$$\mathrm{d}E_c(x) = \sigma_c A(x) \, \mathrm{d}x \tag{3}$$

  where $A(x)$ is the frontal projectile area that contacts the non-crushed laminate. For a spherical projectile, this value varies with the depth of penetration according to

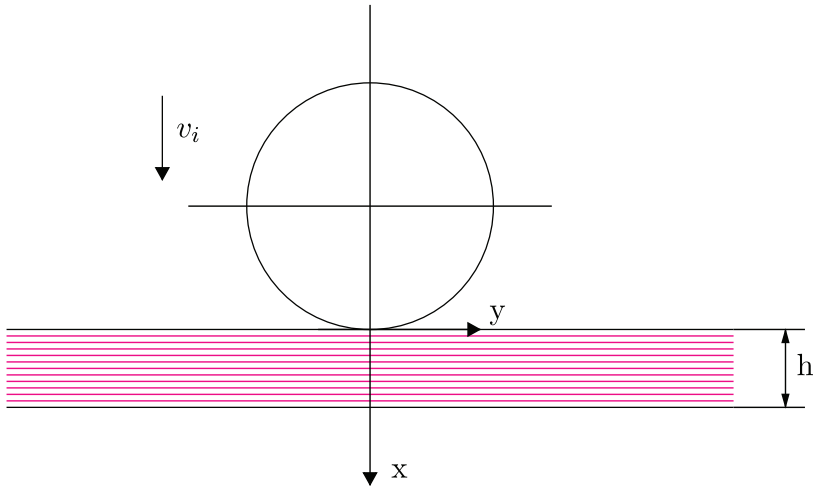

Fig. 1. Projectile and target configuration for null projectile displacement (initial condition).

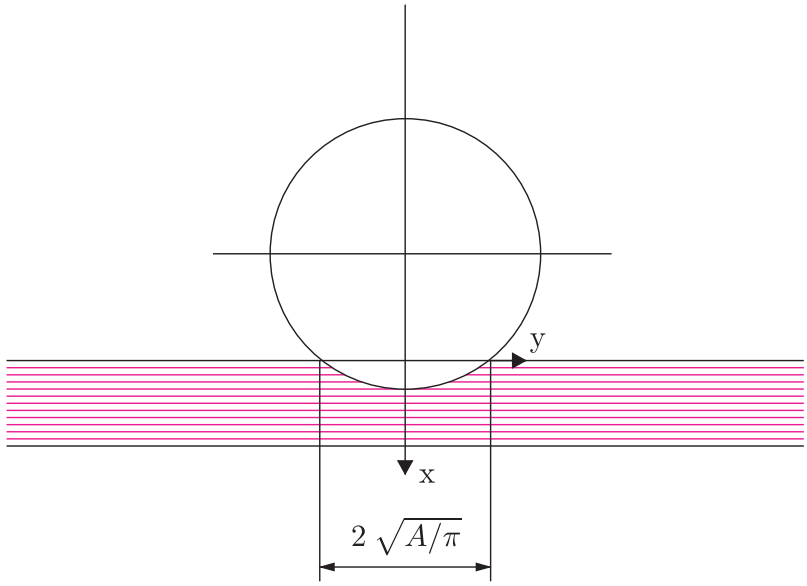

Fig. 2. Sketch of penetration process.

$$A(x) = \begin{cases} \pi(r^2 - (r-x)^2) & \text{if } 0 \leqslant x \leqslant h \\ \pi((r-x+h)^2 - (r-x)^2) & \text{if } h \leqslant x \leqslant r \\ \pi(r-x+h)^2 & \text{if } r \leqslant x \leqslant r+h \\ 0 & \text{if } x \geqslant r+h \end{cases} \tag{4}$$

r being the projectile radius and h the laminate thickness. This energy absorption mechanism disappears when there is no contact between the projectile and the laminate, for $x > h + r$.

- *Energy absorbed by linear momentum transfer*: once the differential laminate volume $A(x)\mathrm{d}x$ has fallen from the composite due to the previous mechanism, it is assumed to accelerate from rest to the projectile velocity. The amount of energy consumed to impel this differential laminate mass, is written as

$$\mathrm{d}E_{\mathrm{m}}(x) = \frac{1}{2}(A(x)\,\mathrm{d}x\rho_{\mathrm{l}})v^2(x) \tag{5}$$

where ρ_l is the laminate density (the term in brackets represents the accelerated mass). Like the previous absorption mechanism, it disappears when $A(x)$ reaches zero.

- *Energy absorbed by tensile fiber failure*: The last two absorption mechanisms describe the plug-in process that appears at impact velocities much higher than that strictly required to perforate the laminate (ballistic limit). At smaller velocities, a third energy dissipation mechanism was observed. Fig. 3 shows an optical microscope image of the transverse plane of a CFRP woven laminate impacted at 100 m/s, which is a velocity slightly below the ballistic limit.
  A crushing breakage was observed in the first plies, while the rest failed through tensile failure in the impact axis. This last zone finally collapsed, creating a 65° troncoconic volume, similar to that observed in brittle materials (such as ceramics) impacted transversally. This kind of breakage appears only when the projectile

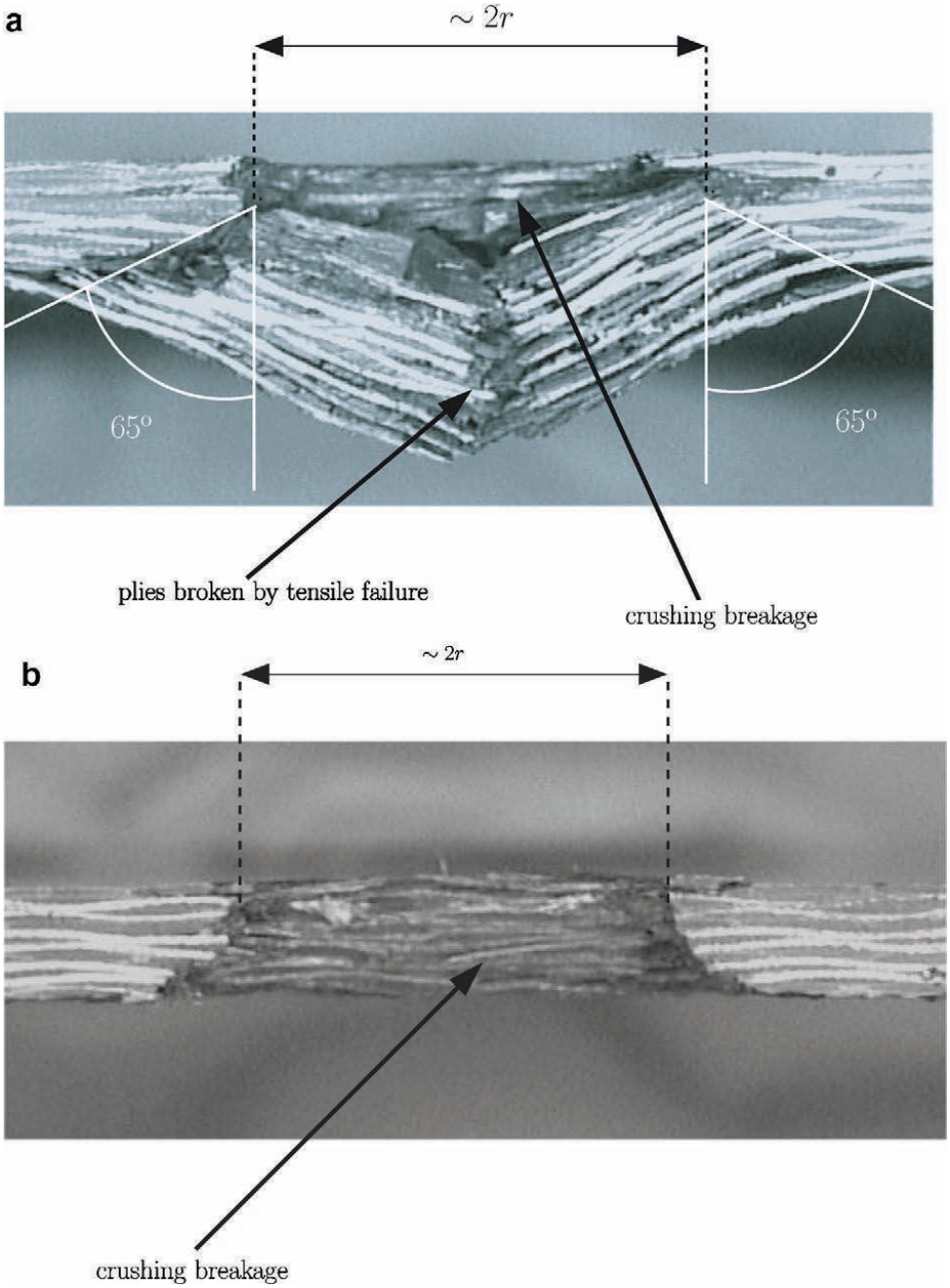

Fig. 3. Cross section view of woven laminate impacted at different velocities (a) 100 m/s, (b) 500 m/s.

velocity is slow, otherwise the non-penetrated plies would not have enough time to break by fiber failure. Numerical simulations of the impact process investigated by López-Puente et al. (2003) shows very good correlation with experimental data (Fig. 4); using these results was found that the time to tensile failure is approximately equal to that needed by the elastic wave to reach the lower face of the laminate and reverse through the total thickness of the plate:

$$t_0 = \frac{2h}{\sqrt{E_3/\rho_1}} \tag{6}$$

E_3 being the elastic modulus through-thickness. The energy differential associated with this failure mechanism was written as

$$\mathrm{d}E_\mathrm{f}(x) = \omega_\mathrm{f}\,\mathrm{d}V \tag{7}$$

in which ω_f is the specific energy and $\mathrm{d}V$ the affected material volume at any $\mathrm{d}x$. Assuming that the fiber behavior is elastic up to failure, the specific energy was estimated as

$$\omega_\mathrm{f} = 2\left(\frac{1}{2}X_\mathrm{t}\varepsilon_\mathrm{f}\right) \tag{8}$$

in which X_t is the tensile strength in direction 1 (and also in 2 on account of the woven configuration) and ε_f is the ultimate strain. The equation is multiplied by two, given the biaxial nature of the tensional field.
The region affected by this kind of failure must be know so as to define the volume $\mathrm{d}V$. An analysis of the transverse section, both in experimental and numerical results (Fig. 4), suggests that the fiber breakage is located in a truncated pyramid, with a semiangle α 65° and its diagonals aligned in the fiber directions. The length of the upper base semidiagonal is r and that of the lower base semidiagonal is L $r + (h - x_0)$ $\tan\alpha$, with x_0 the position of the projectile at t t_0 (Fig. 5). The affected volume for any $\mathrm{d}x$ was described as

$$\mathrm{d}V = 2l^2\,\mathrm{d}x = 2\,\mathrm{d}x(r + (x - x_0)\tan\alpha)^2 \tag{9}$$

and then, the energy absorbed by this mechanism is

$$\mathrm{d}E_\mathrm{f} = X_\mathrm{t}\varepsilon_\mathrm{f}2\,\mathrm{d}x(r + (x - x_0)\tan\alpha)^2 \tag{10}$$

As explained above, this term acts only under certain conditions; a cutdown function, $c_r(x)$, multiplies the last equation annulling it at $t < t_0$, and also when the projectile perforates the laminate.

$$c_r(x) = \begin{cases} 0 & \text{if } 0 < x < x_0 \\ 1 & \text{if } x_0 < x < h \\ 0 & \text{if } x \geqslant h \end{cases} \tag{11}$$

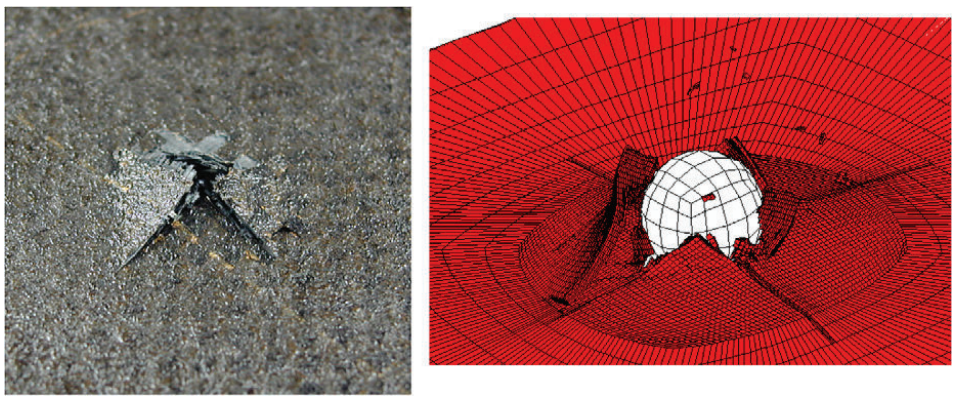

Fig. 4. Images of the laminate lower face impacted at 112 m/s. Experimental test (left) and numerical simulation (right) (López Puente et al. (2003)).

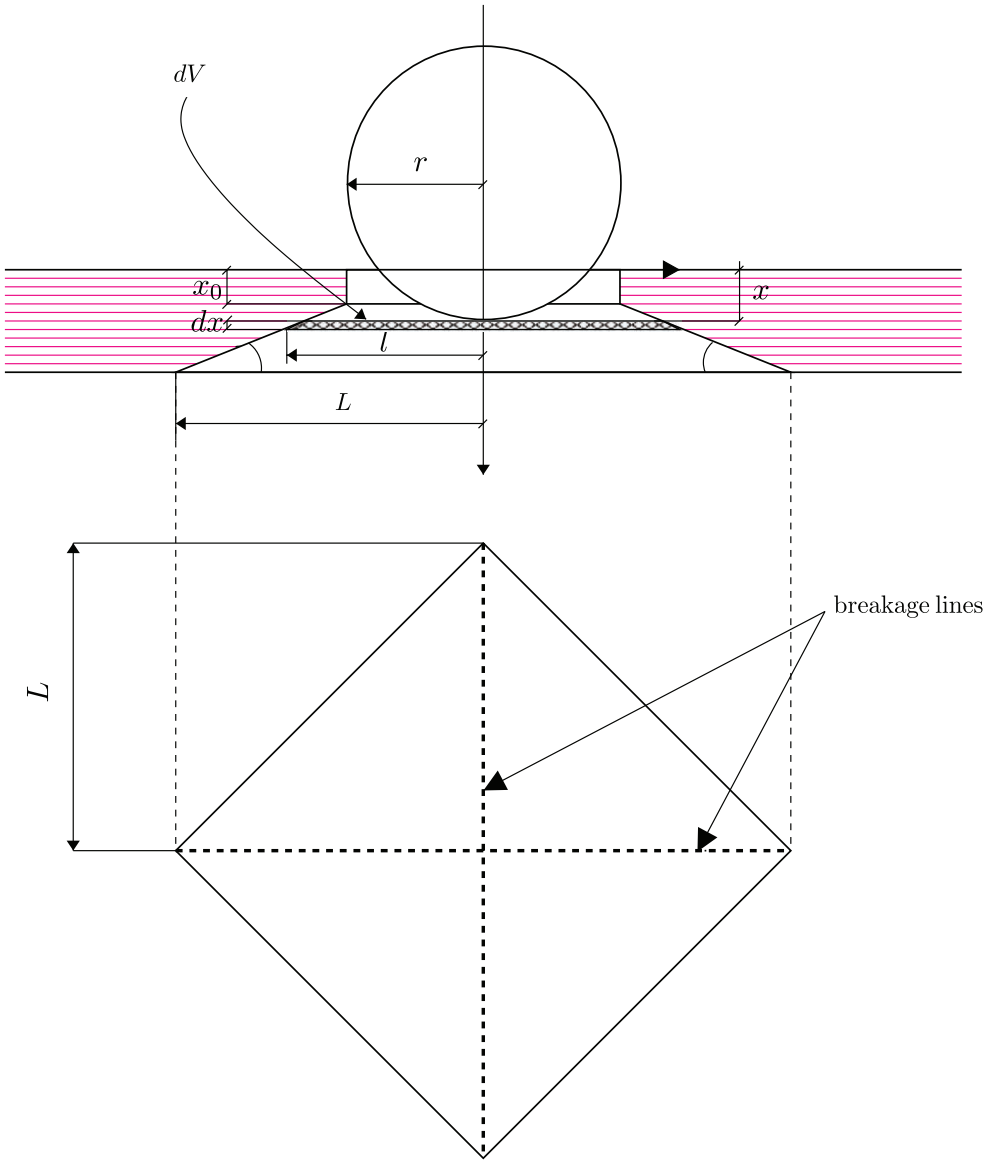

Fig. 5. Fiber failure breakage scheme.

The value of x_0 is determined from the following equation:

$$\int_0^{x_0} \frac{\mathrm{d}\chi}{v(\chi)} = \frac{2h}{\sqrt{E_3/\rho}} \tag{12}$$

χ being a displacement variable, and the unknown function projectile velocity is needed; this difficulty will be solved later.

3. Equation resolution

Once the four differential energy terms are described, they can be grouped as follows:

$$-\frac{1}{2} m_{\mathrm{p}}\, \mathrm{d}(v(x)^2) = \sigma_{\mathrm{c}} A(x)\, \mathrm{d}x + \frac{1}{2}[A(x)\, \mathrm{d}x \rho_{\mathrm{l}}] v^2(x) + 2\, \mathrm{d}x \varepsilon_{\mathrm{f}} X_{\mathrm{t}} (r + (x - x_0) \tan \alpha)^2 c_r(x) \tag{13}$$

Making some simplifications it is possible to obtain the differential equation that solves the problem, with its initial condition:

$$\begin{cases} -\frac{1}{2}m_{\mathrm{p}}\frac{\mathrm{d}v^2}{\mathrm{d}x} = \sigma_{\mathrm{c}}A(x) + \frac{1}{2}(A(x)\rho_{\mathrm{l}})v^2 + 2\varepsilon_{\mathrm{f}}X_{\mathrm{t}}(r + (x - x_0)\tan\alpha)^2 c_r \\ v(0) = v_i \end{cases} \tag{14}$$

Converting the velocity and the projectile displacement into dimensionless variables ($v^* \quad v/v_i$ and $x^* \quad x/h$), using $A(x) \quad A_0 A_{\mathrm{c}}(x^*)$ (where $A_0 \quad \pi r^2$) and then applying the change of variable $w^* \quad v^{*2}$, Eq. (14) leads to

$$\begin{cases} -\frac{\mathrm{d}w^*}{\mathrm{d}x^*} = \frac{2h\sigma_{\mathrm{c}}A_0}{m_{\mathrm{p}}v_i^2}A_{\mathrm{c}} + \frac{hA_0\rho_{\mathrm{l}}}{m_{\mathrm{p}}}w^*A_{\mathrm{c}} + \frac{4h\varepsilon_{\mathrm{f}}X_{\mathrm{t}}r^2}{m_{\mathrm{p}}v_i^2}\left(1 + \left(x^*\frac{h}{r} - \frac{x_0}{r}\right)\tan\alpha\right)^2 c_r(x^*) \\ w^*(0) = 1 \end{cases} \tag{15}$$

This last equation may be numerically solved with any well known method of integration of first order differential equations.

4. Model simplification

A subsequent simplification will be useful in finding a closed-form solution. The first step is to determine the relative importance of each of the energy absorption mechanisms. Table 1 shows the characteristic values of the different parameters involved in the differential equation (15).

Substituting these values it is possible to estimate their relative importance of the terms that appear in the equation as a function of the impact velocity:

$$\begin{cases} R_{\mathrm{ck}} = \frac{2h\sigma_{\mathrm{c}}A_0}{m_{\mathrm{p}}v_i^2} \sim \frac{10^3}{v_i^2} \\ R_{\mathrm{m}} = \frac{hA_0\rho_{\mathrm{l}}}{m_{\mathrm{p}}} \sim 10^{\ 2} \\ R_{\mathrm{fk}} = \frac{4h\varepsilon_{\mathrm{f}}X_{\mathrm{t}}r^2}{m_{\mathrm{p}}v_i^2} \sim \frac{10}{v_i^2} \end{cases}$$

R_{ck} estimates the importance of the energy absorbed by laminate crushing as compared with the projectile initial kinetic energy. R_{m} is the ratio between the laminate mass affected directly by the impact, as compared with the projectile weight, and R_{fk} estimates the energy absorbed by tensile fiber failure, again compared with the projectile initial kinetic energy. The last ratio is always lower than the others at any impact velocity (within the velocity range considered). This fact is the base to simplify the model using a regular perturbation analysis.

To simplify the expression, we rename the equation terms (from now on, asterisks are going to be omitted):

$$\begin{cases} -\frac{\mathrm{d}w}{\mathrm{d}x} = R_{\mathrm{ck}}A_{\mathrm{c}} + R_{\mathrm{m}}A_{\mathrm{c}}w + \varepsilon c_r\left(1 + \frac{hx \quad x_0}{r}\tan\alpha\right)^2 \\ w(0) = 1 \end{cases} \tag{16}$$

Table 1
Characteristic values of the constants that appear in the problem

Variable	Characteristic value
h [m]	10^{-3}
σ_{c} [N/m^2]	10^8
A_0 [m^2]	10^{-5}
m_{p} [kg]	10^{-3}
ρ_{l} [kg/m^3]	10^3
r [m]	10^{-3}
X_{t} [N/m^2]	10^9
ε_{f}	10^{-2}

with the small correction $\varepsilon \quad R_{kf}$. The solution for this equation will be obtained by introducing the expansion $w \quad w_{(0)} + \varepsilon w_{(1)} + O(\varepsilon^2)$; the error will be approximately ε^2. The differential equation for the zero order leads to

$$\begin{cases} -w'_{(0)} = R_{ck} A_c + R_m A_c w_{(0)} \\ w_{(0)}(0) = 1 \end{cases} \tag{17}$$

This differential equation has a simple closed-form solution:

$$w_{(0)}(x) = -\frac{R_{ck}}{R_m} + \left(1 + \frac{R_{ck}}{R_m}\right) \exp(-R_m \widehat{A}_c) \tag{18}$$

where, $\widehat{A}_c(x)$ is the primitive of $A_c(x)$. This solution provides the complete definition of the cut-off function c_r, because for $x < x_0$ the full differential equation (15) and the zero order Eq. (17), are exactly the same. The following equation is used to calculate x_0.

$$\int_0^{x_0} \frac{v_i}{\sqrt{w_{(0)}(\chi)}} \, d\chi = \frac{2h}{\sqrt{E_3/\rho}} \tag{19}$$

The differential equation for the first order term is

$$\begin{cases} -w'_{(1)} = R_m A_c w_{(1)} + c_r \left(1 + \frac{hx \quad x_0}{r} \tan\alpha\right)^2 \\ w_{(1)}(0) = 0 \end{cases} \tag{20}$$

and its solution is

$$w_{(1)}(x) = -\exp(-R_m \widehat{A}_c) \left(\int_0^x c_r \left(1 + \frac{h\kappa - x_0}{r} \tan\alpha\right)^2 \exp(R_m \widehat{A}_c) \, d\kappa \right) \tag{21}$$

An interesting result of this analysis is the closed-form expression for the residual velocity, as a function of geometric parameters, material properties and, of course, impact velocity. The residual velocity is easily determined taking into account the zero order:

$$w_{(0)}(\infty) = \exp(-R_m) \left(1 - \frac{2\sigma_c}{\rho_l v_i^2} (\exp(R_m) - 1)\right) \tag{22}$$

This equation could be very useful for predesign analysis, as a very fast way to obtain a result; it is important however to know the error associated with this expression. Taking into account that fiber failure energy absorbed has been neglected in the zero order solution, the absolute error will be $O(\varepsilon)$ for $w_{(0)}(x)$, as well as for its square root $v_{(0)}$, because:

$$w = w_{(0)} + \varepsilon w_{(1)} \quad \Rightarrow \quad v = (w_{(0)} + \varepsilon w_{(1)})^{1/2} \sim w_{(0)}^{1/2} + \frac{1}{2} \frac{1}{w_{(0)}^{1/2}} \varepsilon w_{(1)} \quad \Rightarrow \quad v = v_{(0)} + \varepsilon \frac{w_{(1)}}{2v_{(0)}} \tag{23}$$

Using Eq. (22) it is possible to obtain the ballistic limit, equaling the residual velocity $w_{(0)}(\infty)$ to zero:

$$v_{bl} = \sqrt{\frac{2\sigma_c}{\rho_l} (\exp(R_m) - 1)} = \sqrt{\frac{2\sigma_c}{\rho_l} \left(\exp\left(\frac{h\rho_l \pi r^2}{m_p}\right) - 1\right)} \tag{24}$$

In this case, the associated error could be estimated from Eq. (22) assuming that the error for w is $O(\varepsilon)$:

$$\exp(-R_m) \left(1 - \frac{2\sigma_c}{\rho_l v_i^2} (\exp(R_m) - 1)\right) + k\varepsilon = 0 \tag{25}$$

where k is a constant that represents the error and $k \sim O(1)$; then:

$$v_{bl} = \left(\frac{2\sigma_c}{\rho_l v_i^2} (\exp(R_m) - 1)\right)^{1/2} \left(\frac{k\varepsilon}{\exp(-R_m)} + 1\right)^{1/2} \tag{26}$$

to calculate the error for the ballistic limit, the value of the second factor must be estimated:

$$\left(\frac{k\varepsilon}{\exp(-R_m)}+1\right)^{1/2} \sim 1+\frac{1}{2}k\varepsilon\exp(R_m) \tag{27}$$

which shows that the error for the ballistic limit is also of ε order.

5. Experimental tests for model validation

To validate the analytical model above described, experimental tests were carried out with woven AGP-193-PW/8552 (AS4 fiber) with 10 plies and a total thickness of 2.2 mm. This configuration is widely used

Table 2
Material ply properties provided by HEXCEL

Property	Value
E_1 [GPa]	68.5
E_2 [GPa]	68.5
E_3 [GPa]	9
G_{12} [GPa]	3.7
v_{12}	0.11
X_t [MPa]	860
X_c [MPa]	795
Y_t [MPa]	860
Y_c [MPa]	795
S_t [MPa]	98
ρ_l [kg/m^3]	1430
ε_f	0.02
σ_c [MPa]	60

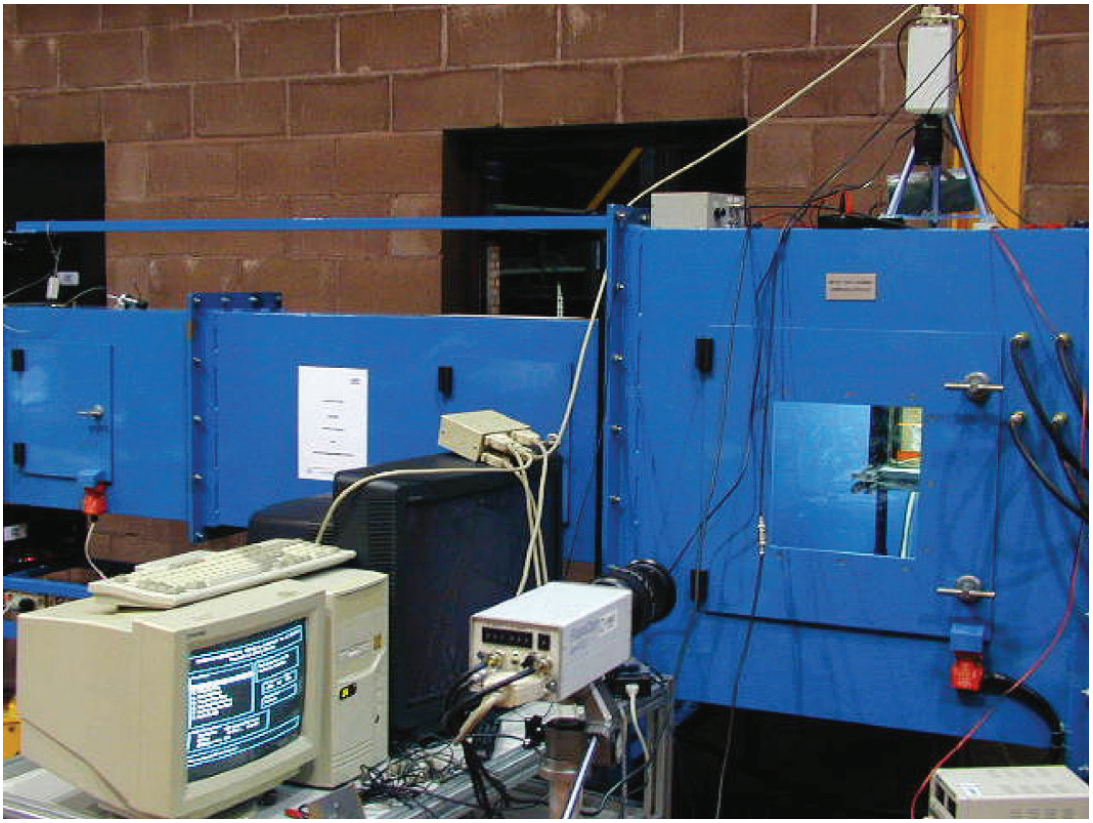

Fig. 6. High speed camera set up.

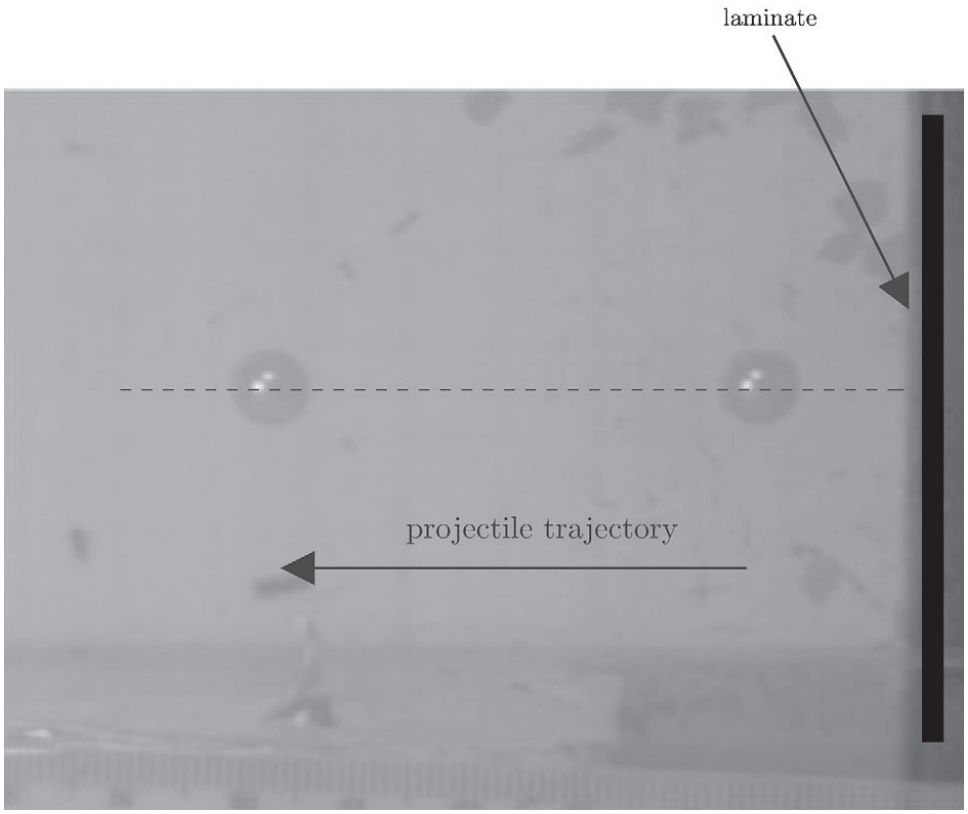

Fig. 7. Example of superposed images of the projectile after perforation of the laminate, obtained with the high speed camera.

in aeronautic and aerospace applications to manufacture structural elements subjected to torsion or shear forces. Its weak delamination under impact loads (López-Puente et al., 2002) makes it a good choice when these are expected in service conditions. The material was provided by SACESA (Spain) from prepregs manufactured by HEXCEL with a volumetric content of fibers of 60%. The elastic and the strength properties of the composite are shown in Table 2. The specimen size was 80×80 mm^2.

A spherical tempered steel projectile (7.5 mm in diameter and 1.73 g of mass) was used. This shape avoids scattered results from possible yaw angle variation during the flight from the gas gun to the specimen. The

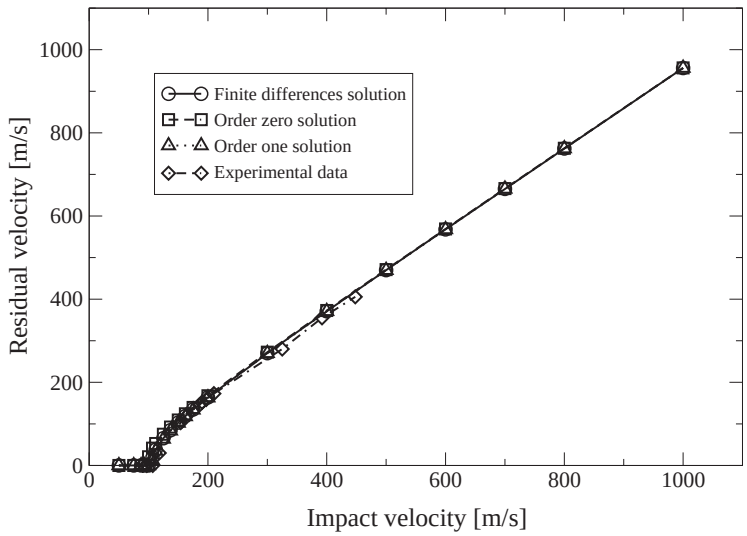

Fig. 8. Residual velocity versus impact velocity.

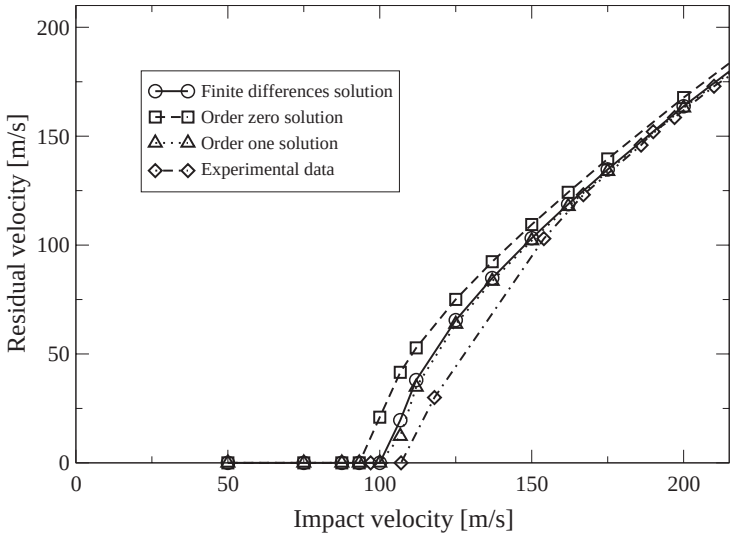

Fig. 9. Residual velocity versus impact velocity, detail.

tempered steel is hard enough to ensure that no plastic deformation will occur during penetration, and this simplifies the analysis because all the energy projectile lost is due to the decrement of its kinetic energy.

A one-stage light gas gun was used to launch the spherical projectiles. This experimental device uses a helium gas bottle at a pressure of 200 bar to impel the fragment up to 500 m/s. It has two photoelectric cells

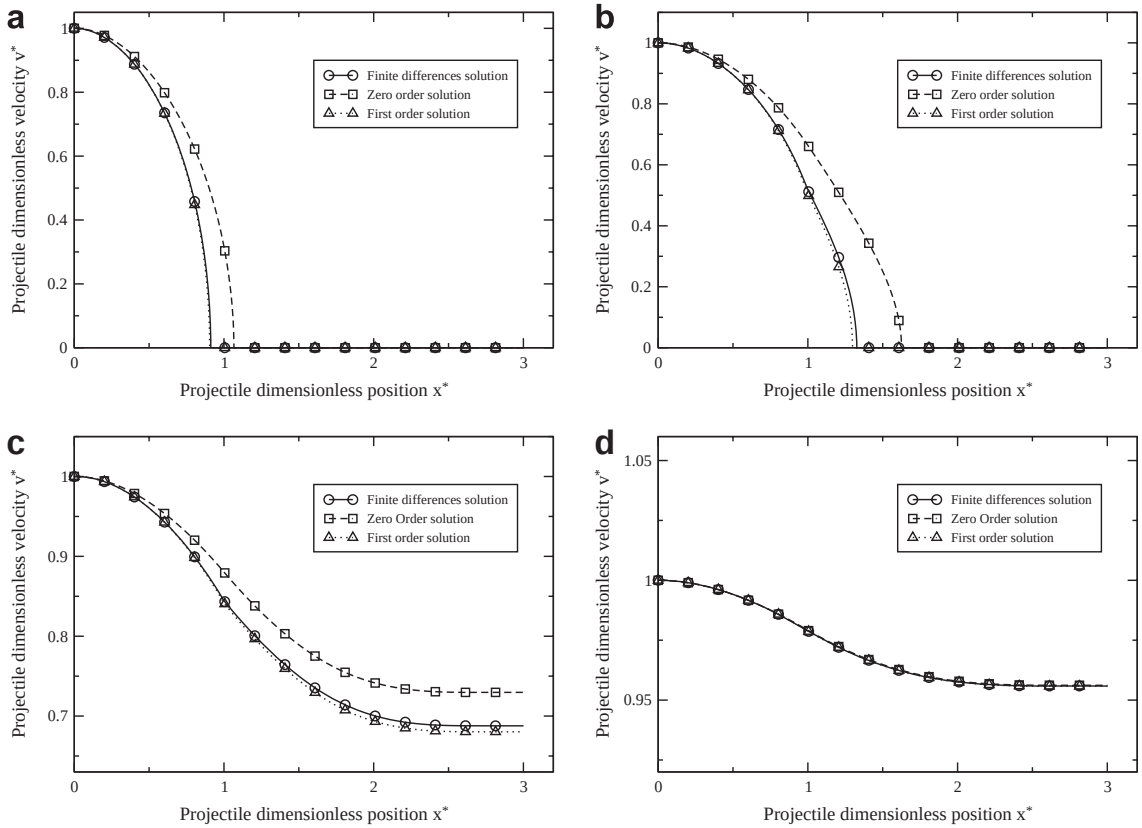

Fig. 10. Dimensionless velocity versus dimensionless displacement for different impact velocities (a) 70 m/s, (b) 90 m/s, (c) 150 m/s, (d) 1000 m/s.

that detect the passing of the projectile, from which the impact velocity is obtained. At the end of the gallery, the projectile reaches an armored chamber ($1 \times 1 \times 1$ m^3) where the specimen is placed.

To measure the residual velocity, two high speed cameras (Flash Cam PCO) were used. Each provides up to ten superimposed images, with an exposure time of 1 μs and a minimum time interval between photos of 1 μs. The gas gun photoelectric cells send a signal that triggers the camera to take the photograph at the appropriate instant. Fig. 6 shows the placing of the two cameras in the impact chamber, one at the side and the other on top. With this set-up the trajectory of the projectile after penetration is accurately determined, for a good measurement of its residual velocity.

An example of the photos is shown in Fig. 7. It is easy to determine the residual velocity using an image treatment software, because the time interval between the two instants is pre-configured in the camera, and the distance between the two spheres is scaled using the bottom rule or using the diameter of the projectile.

6. Results

To validate the analytical model over a wide enough velocity interval, experimental test were done at impact velocities ranging from 60 m/s to 460 m/s. The residual velocity after penetration is the variable used to validate the model. Fig. 8 shows the residual velocity versus the impact velocity, from the experimental data and from results taken from the analytical model: finite differences (using Runge–Kutta), and order one and order zero solution from the perturbation analysis. It is clear that the differences are very small for impact velocities higher that 200 m/s; Fig. 9 presents a detail of the same graph, in the area close to the ballistic limit. Here it is possible to state that the order zero solution overestimates the residual velocity, more than the finite differences solution. Using the result showed in Eq. (23), the expected error associated with the order zero

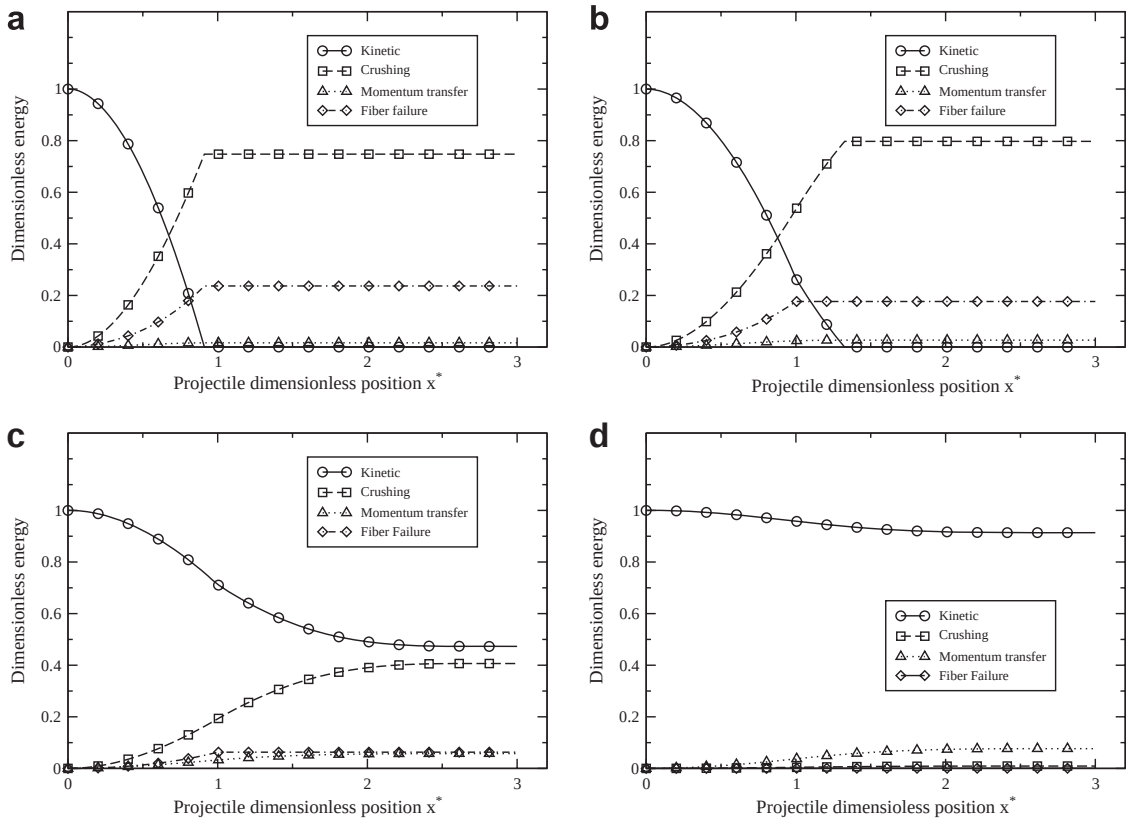

Fig. 11. Dimensionless energy versus dimensionless displacement for different impact velocities (a) 70 m/s, (b) 90 m/s, (c) 150 m/s, (d) 1000 m/s.

solution at velocities close to the ballistic limit (~100 m/s) could be calculated $\varepsilon \sim 12\%$. The actual error between experimental results an this solution is 11%. The order zero solution, from the perturbation analysis, could be use as a very powerful tool for preliminary analysis, due to the fact that a close expression for the ballistic limit is obtained.

Fig. 10 shows the dimensionless projectile velocity as function of its dimensionless position for different impact velocities, using the three results taken from the analytical model. Here it is also clear that finite differential solution and first order solution give almost the same result for every impact velocity. The zero order solution presents good results at high velocities, whereas at low velocities, or around the ballistic limit, differences of 10% could be observed, as was previously estimated.

An other interesting result is to analyze how the laminate absorbs the projectile kinetic energy by the three different mechanism (Fig. 11). For low velocities crushing is the main absorbing energy mechanism, followed by fiber failure; at velocities below 120 m/s the momentum transfer is negligible. As soon as the impact velocity increases, the weight of each term varies, and the momentum transfer rises to a value around the 80% of the total energy absorbed by the laminate for v_i 1000 m/s. This behavior was expected by the fact that this last term is proportional to the square of the projectile velocity. The fiber failure only plays part in the process at low velocities, by the fact that it needs some time to start (cutdown function).

Last analysis summarizes the influence of two most important dimensionless parameters (R_{m} and R_{ck}) in only one graph (Fig. 12a). Here, the ratio between the residual velocity v_r and the impact velocity is plotted in the y axes, and the mass ratio parameter R_{m} in the x axes; the different curves correspond to different values of the crushing–kinetic ratio parameter. It is clear that as R_{m} increases (lighter projectile or heavier laminates), the v_r/v_i decreases for a constant value of R_{ck}. The figure benefits of the dimensionless approach and gathers the information for any impact case consistent with the hypothesis of the model. This way it is possible to obtain $v_r - v_i$ curves (Fig. 12b), frequently used for predesign analysis, by keeping constant R_{m} – and considering that R_{ck} is inversely proportional to the square of the impact velocity.

The family of curves in Fig. 12a smoothly approaches to the one corresponding to R_{ck} 0. This limit value is reached asymptotically when the impact velocity is much higher than the ballistic limit, consequently leading to a proportionally between v_r and v_i at high impact velocity. The asymptotic behavior of the $v_r - v_i$ curve given by the model is also observed experimentally on any projectile-plate impact process. Fig. 12a also shows how the slope of the asymptote of the $v_r - v_i$ curve increases as R_{m} decreases or, in other words, as the mass of

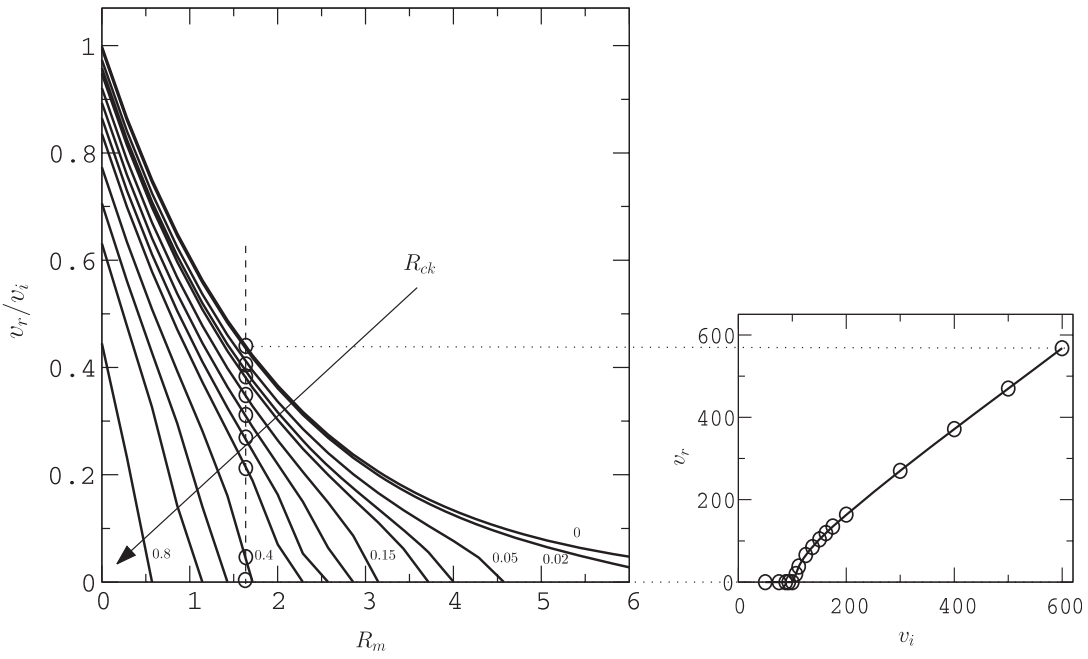

Fig. 12. (a) Left: Influence of R_{m} and R_{ck} on dimensionless residual velocity v_r/v_i. (b) Right: v_r v_i curve for a given value of R_{m}.

the projectile predominates over the mass of the laminate affected by the impact. In the limit case that R_m becomes zero, the residual velocity equals the impact velocity.

7. Conclusions

An analytical model to predict residual velocity after the impact onto a thin carbon/epoxy woven laminate has been developed. The model considers three different energy absorption mechanism for the laminate. Experimental impact test were carried out to validate the model, showing a very good correlation between the results obtained both experimental and numerically, and also demonstrating that the model predicts faithfully the residual velocity of the projectile. A subsequent simplification of the model solution has been done, obtaining a closed-form expression for the residual velocity, which could be useful for predesign purposes.

Acknowledgement

The authors are indebted to the Comisión Interministerial de Ciencia y Tecnología of Spain for the financial support of this work (Project MAT98-0273).

References

Abrate, S., 1991. Impact on laminated composite materials. Appl. Mech. Rev. 44, 155 190.
Abrate, S., 1994. Impact on laminated composite materials: recent advances. Appl. Mech. Rev. 47, 517 544.
Ben Dor, G., Dubinsky, A., Elperin, T., 2002. A model for predicting penetration and perforation of FRP laminates by 3 d impactors. Compos. Struct. 56, 243 248.
Cantwell, W.J., 1988. Influence of target geometry on the high velocity impact response of CFRP. Compos. Struct. 10, 247 265.
Cantwell, W.J., Morton, J., 1985. The ballistic perforation of CFRP. In: Proc. Conf. Impact Polym. Mater.. Guildford Surrey, England, pp. 17/1 17/6.
Cantwell, W.J., Morton, J., 1990. Impact perforation of carbon fibre reinforced plastic. Compos. Sci. Technol. 38, 119 141.
Chen, J.K., Allahdadi, F.A., Carney, T.C., 1997. High velocity impact of graphite/epoxy composite laminates. Compos. Sci. Technol. 57, 1369 1379.
Chocrón, I.S., Rodríguez, J., Martínez, M.A., Sánchez Gálvez, V., 1997. Dynamic tensile testing of aramid and polyethylene fiber composites. Int. J. Impact Eng. 19 (2), 135 146.
Fuji, K., Aoki, M., Kiuchi, N., Tasuda, E., 2002. Impact perforation behavior of cfrps using high velocity stell sphere. Int. J. Impact Eng. 27, 497 508.
Kim, H., Welch, D.A., Kedward, K.T., 2003. Experimental investigation of high velocity ice impacts on woven carbon/epoxy composite panels. Composites A 34, 25 41.
López Puente, J., Zaera, R., Navarro, C., 2002. The effect of low temperatures on the intermediate and high velocity impact response of cfrps. Compos. Part B: Eng. 33 (8), 559 566.
López Puente, J., Zaera, R., Navarro, C., 2003. High energy impact on woven laminates. J. Phys. IV 110, 639 644.
Naik, N.K., Doshi, A.V., 2005. Ballistic impact behavior of thick composites: analytical formulation. AIAA J. 43, 1525 1536.
Naik, N.K., Shrirao, P., Reddy, B.C.K., 2005. Ballistic impact behaviour of woven fabric composites: parametric studies. Mater. Sci. Eng. A Struct. Mater. Prop. Microstruct. Process. 412, 104 116.
Naik, N.K., Shrirao, P., Reddy, B.C.K., 2006. Ballistic impact behaviour of woven fabric composites: formulation. Int. J. Impact Eng. 32, 1521 1552.
Nandlall, D., Williams, K., Viziri, R., 1998. Numerical simulation of the ballistic response of grp plates. Compos. Sci. Technol. 58, 1463 1469.
Navarro, C., 1998. Simplified modelling of the ballistic behaviour of fabrics and fibre reinforce polymeric matrix composites. Key Eng. Mater., 383 400.
Sun, C.T., Potti, S.V., 1996. A simple model to predict residual velocities of thick composite laminates subjected to high velocity impact. Int. J. Impact Eng. 18 (3), 339 353.
Tennyson, R.C., Lamontagne, C., 2000. Hypervelocity impact damage to composites. Composites A 31, 785 794.
Ulven, C., Vaidya, U.K., Hosur, M.V., 2003. Effect of projectile shape during ballistic perforation of VARTM carbon/epoxy composite panels. Compos. Struct. 61, 143 150.
Vasudev, A., Meehlman, M.J., 1987. A comparative study of the ballistic performance of glass reinforced plastic materials. SAMPE Quart. 18 (4), 43 48.
Wen, H.M., 2001. Penetration and perforation of thick FRP laminates. Compos. Sci. Technol. 61, 1163 1172.
Will, M.A., Franz, T., Nurick, G.N., 2002. The effect of laminate stacking sequence of CFRP filament wound tubes subjected to projectile impact. Compos. Struct. 58, 259 270.
Zukas, J.A., 1982. Impact Dynamics. John Wiley and Sons, New York, USA.